JACS JOURNAL OF THE AMERICAN CHEMICAL SOCIETY
Communication
Cite This: J. Am. Chem. Soc. 2019, 141, 5130−5134
pubs.acs.org/JACS

Three-Dimensional Pyrene-Fused *N*-Heteroacenes

Ben-Lin Hu,*[,†] Cunbin An,[†] Manfred Wagner,[†] Georgia Ivanova,[‡] Anela Ivanova,[‡] and Martin Baumgarten*[,†]

[†]Max Planck Institute for Polymer Research, Ackermannweg 10, 55128 Mainz, Germany
[‡]Department of Physical Chemistry, Faculty of Chemistry and Pharmacy, University of Sofia, 1 James Bourchier Avenue, 1164 Sofia, Bulgaria

Supporting Information

ABSTRACT: Four three-dimensional (3D) pyrene-fused *N*-heteroacenes (**P1**−**P4**) are designed and synthesized. From **P1** to **P4**, their lengths are extended in an iterative way, where the thiadiazole unit can be reduced to diamine and the obtained diamines can be further condensed with the diketones with a thiadiazole unit. Compared to their two-dimensional counterparts, the solubility of these 3D pyrene-fused *N*-heteroacenes is improved by this 3D covalent linkage with two-dimensional units. The diameters of **P1**−**P4** are 3.66, 6.06, 8.48 and 10.88 nm, respectively, and these 3D molecules are characterized by ^{1}H, ^{13}C and 2D NMR, MS, UV−vis, PL and CV spectra. Our strategy shows a promising way to large 3D pyrene-fused *N*-heteroacenes.

Since the first *N*-heteroacene was synthesized in the 1960s,[1,2] they have attracted much attention for their outstanding electronic properties and application in organic electronic devices, such as OFETs, OPVs, OLEDs, sensors and as anion radicals.[3−15] Longer and larger *N*-heteroacenes are holy grails to the community of organic electronics and organic chemistry due to their importance for theories and experiments. Therefore, a lot of efforts have been contributed in pursuing such extended and fused heteroaromatics.[3,4,11,12,14] While *N*-heteroacenes up to seven annulated rings can be approached,[16] longer ones usually undergo the Diels−Alder type dimerization during preparation, partially caused by oxidative radical formation.[17−20] In addition, the poor solubility of long *N*-heteroacenes from strong $\pi-\pi$ stacking also blocks their further extension. The insertion of pyrene units into the *N*-heteroacenes is an effective way to further extend the length of *N*-heteroacenes, and usually the obtained long and large *N*-heteroacenes are named pyrene-fused *N*-heteroacenes.[7,11,21−25] We reported pyrene-fused *N*-heteroacenes up to 18 rings terminated by thiadiazoloquinoxaline (TQ) units stabilizing it structurally with pyrene contributing to stabilizing the structure and TQ as ending groups to ensure low LUMO energy levels.[25] More interestingly, nanoribbon-like layered structures by the adjacent thiadiazole units were observed in the crystals which enhances the charge transport.[25−28] Well soluble pyrene-fused heteroacenes up to 30 rings with a size up to 7.7 nm were reported, too, using triisobutylsilyl (TIBS) to replace triisopropylsilyl (TIPS) in the side chain and large ketal as terminal units, which block the condense packing and thus result in poor charge transport.[29] Above all, new ways for further extending the length of pyrene-fused *N*-heteroacenes are crucially needed.

The integration of 2D building blocks, such as nanographenes and graphene sheets, into 3D hierarchical architectures is an effective way to extend the size and avoid aggregation of 2D structures.[30−33] This has attracted much attention in view of nanomaterials and their exploration of advanced properties of individual 2D nanoscale structures for practical applications in energy storage and conversion, environmental remediation and catalysis.[30−33] In addition, the newly produced 3D structures are able to avoid the irreversible aggregation resulting from the individual 2D nano building blocks and their restacking due to the strong $\pi-\pi$ stacking and van der Waals forces between the planar planes of 2D sheets which lead to the loss of the large surface area, thus limiting the potential application of the 2D materials.[34−36] Therefore, learning how to construct 3D nanostructures to further extend the size of pyrene-fused *N*-heteroacenes can be very advantageous.

Herein, we report three-dimensionally extended N-doped pyrene-fused heteroacenes (**P1**−**P4**) obtained by organic synthesis. As shown in Figure 1, the 3D pyrene-fused heteroacenes with triptycene core with three wings, which has a length of ∼1.7 nm, are based on our previous TQ containing pyrene-fused *N*-heteroacene unit.[25] The average diameters of the 3D pyrene-fused heteroacenes are 3.66, 6.06, 8.48 and 10.88 nm for **P1**−**P4**, respectively. It should be noted that **P4** is the largest pyrene-fused *N*-heteroacene reported to date.[25,29,37−41] These 3D pyrene-fused *N*-heteroacenes show good solubility and overcome the aggregation by the three-dimensional structure. The good solubility enables the full characterization of these 3D pyrene-fused heteroacenes by ^{1}H and ^{13}C NMR spectroscopy, high-resolution mass spectrometry, absorption and photoluminescence spectroscopy, and cyclic voltammetry. Our exploration on 3D pyrene-fused *N*-heteroacenes supplies a new perspective to large 3D molecules for electronic, optoelectronic and energy storage and conversion devices.

As shown in Scheme S1, the intermediate **A** is synthesized by the condensation of *tert*-butyl pyrene tetraketone (**S1**)[24,25,42] with TIPS acetylene benzothiadiazole diamine (**S2**)[27] in $CHCl_3$/HOAc. The intermediate **A** can be readily

Received: January 29, 2019
Published: March 12, 2019

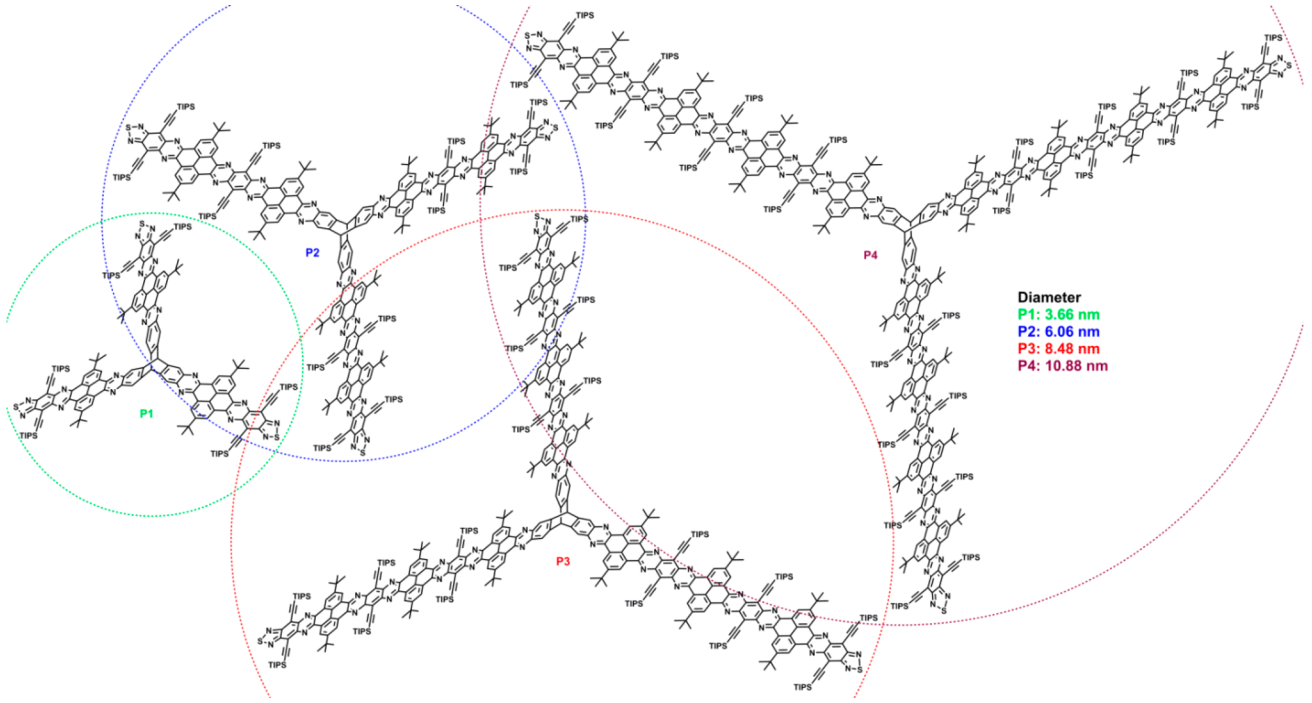

Figure 1. Chemical structures of **P1**−**P4**.

Scheme 1. Synthesis of P1−**P4**

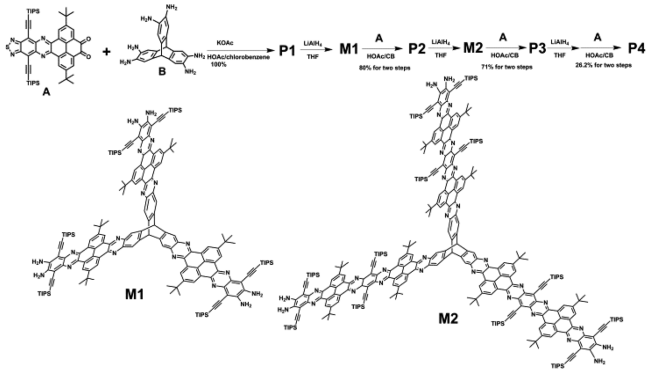

soluble in dichloromethane, $CHCl_3$, tetrahydrofuran, etc., so it can be characterized by the ^1H and ^{13}C NMR spectra (Figures S1 and S2). The synthesis of 3D pyrene-fused *N*-heteroacenes (**P1**−**P4**) is depicted in Scheme 1. **P1** was synthesized by the condensation of the intermediate **A** and hexamine triptycene hydrochloride salt **B** refluxing in the mixed solvents (cholorobenzene/acetic acid) and KOAc. An iterative way is employed to further increase the length of nanoribbons to **P2**−**P4**, where the thiadiazole units are reduced by large excess of $LiAlH_4$ (60 equiv for **P1**, 300 equiv for **P2** and 450 equiv for **P3**) in THF to diamines, and then the obtained diamines are condensed with **A** to produce **P2**-**P4**. Compared to their linear counterparts (18 rings can only be soluble in hot *o*-dichlorobenzene),[25] **P1**−**P4** (**P4** with 22 rings) show good solubility in dichloromethane, THF, chlorobenzene and tetrachloroethane, but the solubility is decreased from **P1** to **P4**. Therefore, **P1**−**P3** can be characterized by ^1H, ^{13}C and 2D (HSQC, NOESY) NMR (**P1** in CD_2Cl_2, **P2** in THF-d_8 at room temperature, **P3** at 120 °C and **P4** at 140 °C in $C_2D_2Cl_4$ (Figures S3−S17). 35 mg of **P3** (1125 atoms, 55 carbons with different chemical shifts) in 0.5 mL $C_2D_2Cl_4$ and more than

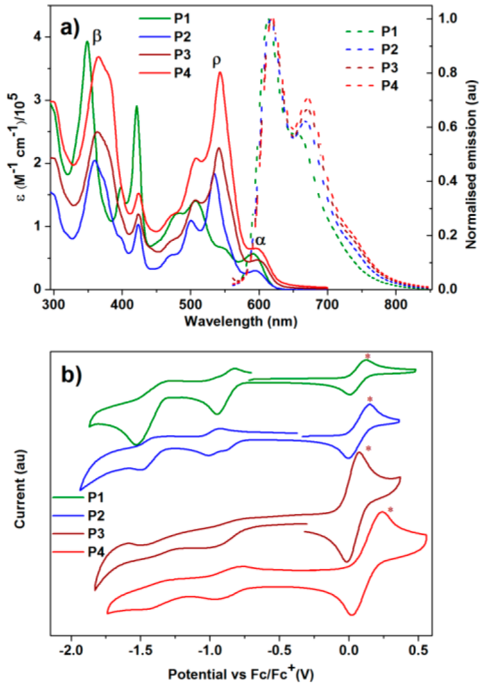

Figure 2. UV−vis absorption (10^{-6} M, solid lines) and fluorescence emission (10^{-6} M, dash lines) in THF and (b) the cyclic voltammograms of **P1**−**P4** in an 0.1 M *n*-Bu_4NPF_6 solution in THF at a scan rate of 100 mV s^{-1} with ferrocene (ferrocene peaks are marked with purple stars, and occur at positive potential) as internal standard.

50 000 scans were used to gain resolved ^{13}C NMR spectrum at 140 °C. However, no ^{13}C NMR with high enough intensity was obtained due to too many atoms in **P4** (1501 atoms, 69 carbons with different chemical shifts predicted theoretically), whereas the NOESY indicted a clear structure of **P4** (Figures S18 and S19). In addition, the HRMS (Figures S20−S24),

DOI: 10.1021/jacs.9b01082
J. Am. Chem. Soc. 2019, 141, 5130−5134

Table 1. Photophysical and Electrochemical Data and B3LYP/6-31G Energy Levels of P1−P4

compd	λ_{abs}^{0-0} (nm)	λ_{onset}^{0-1} (nm)	E_{gap} (eV)[a]	λ_{em} (nm)	$E_{onset,red1}$ (V)[b]	EA (eV)[c]	$E_{LUMO,DFT}$ (eV)	$E_{HOMO,DFT}$ (eV)
P1	591	618	2.00	614	−0.81	3.99	−3.67	−6.15
P2	593	623	1.99	617	−0.78	4.02	−3.68	−6.13
P3	596	629	1.97	617	−0.75	4.05	−3.69	−6.08
P4	598	632	1.96	617	−0.72	4.08	−3.68	−6.06

[a]Estimated from absorption onset. [b]Measured in *n*-Bu_4NPF_6 solution in CH_2Cl_2 with a scan rate of 100 mV/s, and ferrocene as internal standard. [c]Estimated from $E_{onset,red}$, and energy of Fc/Fc^+ is assumed at −4.8 eV relative to vacuum.[49]

GPC (Figure S25) and elemental analysis results also confirm the pure and exact target structures we obtained for **P1−P4**.

Much effort was invested to grow crystals of **P1−P4** in different solvents under various conditions; however, no crystal with high enough quality for single-crystal X-ray diffraction analysis was obtained. Thus, computational simulation was employed to investigate the geometry, molecular orbitals, optical and electronic properties of **P1−P4**. DFT calculations were used, namely B3LYP/6-31G in vacuum and B3LYP/6-31G(d) in implicit THF solvent.[43] There are too many atoms in the side chains, which should not markedly affect the geometry of the π-conjugated system and, hence, the molecular orbitals and optical and electronic properties of **P1−P4**. Since those atoms will consume too much computational resource, all the side chains were omitted to simplify the calculations. As shown in Figures S26−S29, rigid and conjugated backbones are observed in **P1**; however, the backbone becomes more and more flexible as the arm length increased in **P2−P4**, which means all the atoms of the backbone of each arm are not necessarily in the same plane but a little bit bent and twisted, such that each arm is not a pure 2D structures but has 2.5D character. This feature is preserved both in vacuum and in THF. Such an effect was also observed in extended graphene sheets.[44] Because of this flexibility, the three arms are not distributed equally in space but, nevertheless, have similar length with a radius of 1.83, 3.03, 4.24 and 5.44 nm, providing averaged wingspans of 3.16 ± 0.05 nm, 5.16 ± 0.02 nm, 7.34 ± 0.15 nm and 9.41 ± 0.35 nm for **P1−P4**, respectively. According to the calculations, the twist of the arms also impedes the packing of the molecules, which explains the poor crystallinity of these molecules. In addition, the possible large porous structures (**P1** as an example shown in Figure S30) are not stable to support the backbone of the crystals. Otherwise, it will collapse.

The DFT LUMO energy levels are −3.67, −3.68, −3.69 and −3.68 eV for **P1−P4**, respectively, while the HOMO energies varied from −6.15, −6.13, −6.08 and −6.06 eV in this series. Expectedly, the HOMO and LUMO energy levels of **P1−P4** are 3-fold degenerate, as illustrated in Figures S31 to S34. The electron densities of the LUMOs are mainly located on the TQ and pyrazine units. As we expected, the electronic communication along the system are blocked by the pyrene unit. This, however, is not true for **P1**. There, the LUMOs are delocalized also on the pyrene unit in two of the arms. The major change upon elongation is in the HOMOs. From being delocalized over the outer part of the arms in **P1**, they move toward the core in **P3**, thereby extending the degree of delocalization. In spite of this change, the energy of the frontier orbitals is affected very slightly from extension of the size. The calculated electronic absorption transitions of **P1** are shown in Figure S33.

The experimental absorption profiles of **P1−P4** in THF (10^{-6} M) are shown in Figure 2a. There are three bands in the spectra, corresponding to β, ρ and α band, respectively, which agrees with Clar's nomenclature in the polycyclic aromatic hydrocarbons (PAH).[45,46] The first bands in the UV−vis spectra originate from the $\pi-\pi$ transition, and the second bands can be attributed to the n−π transition of the conjugated aromatic backbones.[47] From **P1** to **P4**, small red-shifts are observed, which are similar to our previous results in linear graphene nanoribbons[25] and agree with the computational result (Figure S33). The third bands in **P1−P4** can be assigned to the 0−1 and 0−0 transitions.[48] Because of the range of conjugation, the intensity of the β band in **P1** is stronger than that of the other two bands, while as the length increasing for **P2−P4**, the intensity of the ρ band is stronger than that of the β and α bands in **P1**, and the intensity increase from **P2** to **P4**. There are four peaks in the ρ and α band, and the peaks are slightly red-shifted from **P1** to **P4**. The TD-DFT calculations show that the transition from the α band of **P1** corresponds to charge transfer from the pyrene-N-doped acene core of the molecule to the three terminal TQs (Figure S34). The first two transitions of the ρ band originate from exchange of electron density within the arms, either within the TQ units or from pyrene to them. The onset absorption of **P1−P4** is 620, 623, 629 and 633 nm, respectively, which are similar to the DFT calculation results, and the corresponding energy gaps of **P1−P4** are 2.00, 1.99, 1.97 and 1.96 eV, respectively.

The normalized photoluminescence (PL) spectra of **P1−P4** in THF (10^{-6} M) are shown as the dash lines in Figure 2a. Similar emission profiles that have a maximum emission (614 nm for **P1** and 617 nm for **P2−P4**) and vibronic shoulder peaks (654 nm for **P1**, 667 for **P2**, 670 for **P3** and 671 nm for **P4**) are observed in **P1−P4**. Remarkably, the emission bands of **P1−P4** expand into the NIR region, up to 850 nm. Because of the rigid 3D conjugated backbones, small Stokes shift of 23, 24, 21 and 19 nm for **P1−P4** were observed, respectively, which are smaller than that of their linear counterparts, and agrees with their higher rigidity of 2.5D structures than those of their linear counterparts.[25]

The cyclic voltammetry (CV) curves of **P1−P4** in THF with tetrabutylammonium hexafluorophosphate (*n*-Bu_4PF_6) as electrolyte (0.1 M) are shown in Figure 2b. In the negative direction, two quasi-reversible reduction peaks are observed. The onset voltages of the reduction peaks are −0.81, −0.78, −0.75 and −0.72 V for **P1−P4**, respectively. The corresponding LUMOs are −3.97, −4.01, −4.04 and −4.08 eV for **P1−P4**, respectively. Though the electronic communication is usually blocked by pyrene, the LUMO energy levels slightly decrease from **P1** to **P4**, which agrees with the DFT calculations. All of these data are summarized in Table 1.

In conclusion, three-dimensional pyrene-fused *N*-heteroacenes with a size approaching 11 nm were designed, synthesized and fully characterized by ^1H, ^{13}C and 2D NMR spectra, MS, UV−vis, PL and CV. These 3D NRs possess low LUMO energy levels and are investigated by DFT simulations.

DOI: 10.1021/jacs.9b01082
J. Am. Chem. Soc. 2019, 141, 5130−5134

Our results provide the perspective of 3D pyrene-fused *N*-heteroacenes obtained by organic synthesis for the promising application in organic electronics and energy conversion.

■ ASSOCIATED CONTENT

Supporting Information

The Supporting Information is available free of charge on the ACS Publications website at DOI: 10.1021/jacs.9b01082.

Experimental details, characterization data, NMR spectra and MALDI-TOF MS of all new compounds, and DFT structures, frontier molecular orbitals, and absorption spectra (PDF)

■ AUTHOR INFORMATION

Corresponding Authors

*hubenlin@mpip-mainz.mpg.de

*martin.baumgarten@mpip-mainz.mpg.de

ORCID

Ben-Lin Hu: 0000-0001-6576-2485

Cunbin An: 0000-0001-6019-2700

Anela Ivanova: 0000-0001-6220-7961

Martin Baumgarten: 0000-0002-9564-4559

Notes

The authors declare no competing financial interest.

■ ACKNOWLEDGMENTS

This work was supported by the SFB-TR49 and the EU programme Horizon 2020 under Project Materials Networking (grant agreement 692146). We thank Jutta Schnee for the Maldi-TOF MS measurement and Stefan Spang for the high temperature NMR measurements. Ben-Lin Hu gratefully acknowledges the Alexander von Humboldt Stiftung for a research fellowship.

■ REFERENCES

(1) Kummer, F.; Zimmermann, H. Über die Elektronenspektren linearer Diaza- und Tetraaza-Acene. *Ber. Bunsen-Ges.* **1967**, *71*, 1119−1125.

(2) Leete, E.; Ekechukwu, O.; Delvigs, P. Lineat Indanthrone and Related Phenazines. *J. Org. Chem.* **1966**, *31*, 3734−3739.

(3) Bunz, U. H. F. The Larger Linear N-Heteroacenes. *Acc. Chem. Res.* **2015**, *48*, 1676−1686.

(4) Bunz, U. H. F.; Engelhart, J. U.; Lindner, B. D.; Schaffroth, M. Large N-heteroacenes: new tricks for very old dogs? *Angew. Chem., Int. Ed.* **2013**, *52*, 3810−3821.

(5) Endres, A. H.; Schaffroth, M.; Paulus, F.; Reiss, H.; Wadepohl, H.; Rominger, F.; Krämer, R.; Bunz, U. H. F. Coronene-Containing N-Heteroarenes: 13 Rings in a Row. *J. Am. Chem. Soc.* **2016**, *138*, 1792−1795.

(6) Ganschow, M.; Koser, S.; Hahn, S.; Rominger, F.; Freudenberg, J.; Bunz, U. H. F. Dibenzobarrelene-Based Azaacenes: Emitters in Organic Light-Emitting Diodes. *Chem. - Eur. J.* **2017**, *23*, 4415−4421.

(7) Gu, P.-Y.; Wang, Z.; Liu, G.; Yao, H.; Wang, Z.; Li, Y.; Zhu, J.; Li, S.; Zhang, Q. Synthesis, Full Characterization, and Field Effect Transistor Behavior of a Stable Pyrene-Fused N-Heteroacene with Twelve Linearly Annulated Six-Membered Rings. *Chem. Mater.* **2017**, *29*, 4172.

(8) Ji, L.; Friedrich, A.; Krummenacher, I.; Eichhorn, A.; Braunschweig, H.; Moos, M.; Hahn, S.; Geyer, F. L.; Tverskoy, O.; Han, J.; Lambert, C.; Dreuw, A.; Marder, T. B.; Bunz, U. H. F. Preparation, Properties, and Structures of the Radical Anions and Dianions of Azapentacenes. *J. Am. Chem. Soc.* **2017**, *139*, 15968−15976.

(9) Lami, V.; Leibold, D.; Fassl, P.; Hofstetter, Y. J.; Becker-Koch, D.; Biegger, P.; Paulus, F.; Hopkinson, P. E.; Adams, M.; Bunz, U. H. F.; et al. *N*-Heteroacenes as a New Class of Non-Fullerene Electron Acceptors for Organic Bulk-Heterojunction. *Photovoltaic Devices Solar RRL* **2017**, *1*, 1700053.

(10) Leibold, D.; Lami, V.; Hofstetter, Y. J.; Becker-Koch, D.; Weu, A.; Biegger, P.; Paulus, F.; Bunz, U. H. F.; Hopkinson, P. E.; Bakulin, A. A.; Vaynzof, Y. Triptycenyl-phenazino-thiadiazole as acceptor in organic bulk-heterojunction solar cells. *Org. Electron.* **2018**, *57*, 285−291.

(11) Mateo-Alonso, A. Pyrene-fused pyrazaacenes: from small molecules to nanoribbons. *Chem. Soc. Rev.* **2014**, *43*, 6311−6324.

(12) Miao, Q. Ten Years of N-Heteropentacenes as Semiconductors for Organic Thin-Film Transistors. *Adv. Mater.* **2014**, *26*, 5541−5549.

(13) Xu, X.; Yao, Y.; Shan, B.; Gu, X.; Liu, D.; Liu, J.; Xu, J.; Zhao, N.; Hu, W.; Miao, Q. Electron Mobility Exceeding 10 cm2 V−1 s−1 and Band-Like Charge Transport in Solution-Processed n-Channel Organic Thin-Film Transistors. *Adv. Mater.* **2016**, *28*, 5276−5283.

(14) Gu, P.-Y.; Wang, Z.; Zhang, Q. Azaacenes as active elements for sensing and bio applications. *J. Mater. Chem. B* **2016**, *4*, 7060−7074.

(15) Zhang, Y.-D.; Wu, Y.; Xu, Y.; Wang, Q.; Liu, K.; Chen, J.-W.; Cao, J.-J.; Zhang, C.; Fu, H.; Zhang, H.-L. Excessive Exoergicity Reduces Singlet Exciton Fission Efficiency of Heteroacenes in Solutions. *J. Am. Chem. Soc.* **2016**, *138*, 6739−6745.

(16) Engelhart, J. U.; Tverskoy, O.; Bunz, U. H. F. A Persistent Diazaheptacene Derivative. *J. Am. Chem. Soc.* **2014**, *136*, 15166−15169.

(17) Xia, D.; Guo, X.; Chen, L.; Baumgarten, M.; Keerthi, A.; Müllen, K. Layered Electron Acceptors by Dimerization of Acenes End-Capped with 1,2,5-Thiadiazoles. *Angew. Chem., Int. Ed.* **2016**, *55*, 941−944.

(18) Inoue, Y.; Sakamaki, D.; Tsutsui, Y.; Gon, M.; Chujo, Y.; Seki, S. Hash-Mark-Shaped Azaacene Tetramers with Axial Chirality. *J. Am. Chem. Soc.* **2018**, *140*, 7152−7158.

(19) Das, A.; Pinheiro, M.; Machado, F. B. C.; Aquino, A. J. A.; Lischka, H. Tuning the Biradicaloid Nature of Polycyclic Aromatic Hydrocarbons: The Effect of Graphitic Nitrogen Doping in Zethrenes. *ChemPhysChem* **2018**, *19*, 2492−2499.

(20) Zeng, W.; Phan, H.; Herng, T. S.; Gopalakrishna, T. Y.; Aratani, N.; Zeng, Z.; Yamada, H.; Ding, J.; Wu, J. Rylene Ribbons with Unusual Diradical Character. *Chem.* **2017**, *2*, 81−92.

(21) Cortizo-Lacalle, D.; Pertegas, A.; Melle-Franco, M.; Bolink, H. J.; Mateo-Alonso, A. Pyrene-fused bisphenazinothiadiazoles with red to NIR electroluminescence. *Org. Chem. Front.* **2017**, *4*, 876−881.

(22) Wang, C.; Zhang, J.; Long, G.; Aratani, N.; Yamada, H.; Zhao, Y.; Zhang, Q. Synthesis, Structure, and Air-stable N-type Field-Effect Transistor Behaviors of Functionalized Octaazanonacene-8,19-dione. *Angew. Chem., Int. Ed.* **2015**, *54*, 6292−6296.

(23) Marco, A. B.; Gozalvez, C.; Olano, M.; Sun, X.; Atxabal, A.; Melle-Franco, M.; Hueso, L. E.; Mateo-Alonso, A. Bis-(triisopropylsilylethynyl)-substituted pyrene-fused tetraazaheptacene: synthesis and properties. *Phys. Chem. Chem. Phys.* **2016**, *18*, 11616−11619.

(24) Wang, Z.; Gu, P.; Liu, G.; Yao, H.; Wu, Y.; Li, Y.; Rakesh, G.; Zhu, J.; Fu, H.; Zhang, Q. A large pyrene-fused N-heteroacene: fifteen aromatic six-membered rings annulated in one row. *Chem. Commun.* **2017**, *53*, 7772−7775.

(25) Hu, B.-L.; Zhang, K.; An, C.; Schollmeyer, D.; Pisula, W.; Baumgarten, M. Layered Thiadiazoloquinoxaline-Containing Long Pyrene-Fused N-Heteroacenes. *Angew. Chem., Int. Ed.* **2018**, *57*, 12375−12379.

(26) An, C.; Guo, X.; Baumgarten, M. Highly Ordered Phenanthroline-Fused Azaacene. *Cryst. Growth Des.* **2015**, *15*, 5240−5245.

(27) An, C.; Zhou, S.; Baumgarten, M. Condensed Derivatives of Thiadiazoloquinoxaline as Strong Acceptors. *Cryst. Growth Des.* **2015**, *15*, 1934−1938.

(28) Hu, B.-L.; Zhang, K.; An, C.; Pisula, W.; Baumgarten, M. Thiadiazoloquinoxaline-Fused Naphthalenediimides for n-Type Or-

DOI: 10.1021/jacs.9b01082
J. Am. Chem. Soc. 2019, 141, 5130−5134

ganic Field-Effect Transistors (OFETs). *Org. Lett.* **2017**, *19*, 6300−6303.
(29) Cortizo-Lacalle, D.; Mora-Fuentes, J. P.; Strutynski, K.; Saeki, A.; Melle-Franco, M.; Mateo-Alonso, A. Monodisperse N-Doped Graphene Nanoribbons Reaching 7.7 Nanometers in Length. *Angew. Chem., Int. Ed.* **2018**, *57*, 703−708.
(30) Sudeep, P. M.; Narayanan, T. N.; Ganesan, A.; Shaijumon, M. M.; Yang, H.; Ozden, S.; Patra, P. K.; Pasquali, M.; Vajtai, R.; Ganguli, S.; Roy, A. K.; Anantharaman, M. R.; Ajayan, P. M. Covalently Interconnected Three-Dimensional Graphene Oxide Solids. *ACS Nano* **2013**, *7*, 7034−7040.
(31) Li, D.; Kaner, R. B. Graphene-Based Materials. *Science* **2008**, *320*, 1170−1171.
(32) Wu, Z.-S.; Yang, S.; Sun, Y.; Parvez, K.; Feng, X.; Müllen, K. 3D Nitrogen-Doped Graphene Aerogel-Supported Fe_3O_4 Nanoparticles as Efficient Electrocatalysts for the Oxygen Reduction Reaction. *J. Am. Chem. Soc.* **2012**, *134*, 9082−9085.
(33) Romo-Herrera, J. M.; Terrones, M.; Terrones, H.; Dag, S.; Meunier, V. Covalent 2D and 3D Networks from 1D Nanostructures: Designing New Materials. *Nano Lett.* **2007**, *7*, 570−576.
(34) Narita, A.; Wang, X.-Y.; Feng, X.; Müllen, K. New advances in nanographene chemistry. *Chem. Soc. Rev.* **2015**, *44*, 6616−6643.
(35) Saathoff, J. D.; Clancy, P. Simulation of Graphene Nanoribbon Aggregation and Its Mediation by Edge Decoration. *Carbon* **2017**, *115*, 154−161.
(36) Fan, Z.; Yan, J.; Zhi, L.; Zhang, Q.; Wei, T.; Feng, J.; Zhang, M.; Qian, W.; Wei, F. A Three-Dimensional Carbon Nanotube/Graphene Sandwich and Its Application as Electrode in Supercapacitors. *Adv. Mater.* **2010**, *22*, 3723−3728.
(37) Sisto, T. J.; Zhong, Y.; Zhang, B.; Trinh, M. T.; Miyata, K.; Zhong, X.; Zhu, X. Y.; Steigerwald, M. L.; Ng, F.; Nuckolls, C. Long, Atomically Precise Donor−Acceptor Cove-Edge Nanoribbons as Electron Acceptors. *J. Am. Chem. Soc.* **2017**, *139*, 5648−5651.
(38) Kohl, B.; Bohnwagner, M. V.; Rominger, F.; Wadepohl, H.; Dreuw, A.; Mastalerz, M. Attractive Dispersion Interactions Versus Steric Repulsion of *tert*-Butyl groups in the Crystal Packing of a D_{3h}-Symmetric Tris(quinoxalinophenanthrophenazine). *Chem. - Eur. J.* **2016**, *22*, 646−655.
(39) Kohl, B.; Rominger, F.; Mastalerz, M. Crystal Structures of a Molecule Designed Not To Pack Tightly. *Chem. - Eur. J.* **2015**, *21*, 17308−17313.
(40) Kohl, B.; Rominger, F.; Mastalerz, M. Rigid π-Extended Triptycenes via a Hexaketone Precursor. *Org. Lett.* **2014**, *16*, 704−707.
(41) Zhang, C.; Liu, Y.; Xiong, X.-Q.; Peng, L.-H.; Gan, L.; Chen, C.-F.; Xu, H.-B. Three-Dimensional Nanographene Based on Triptycene: Synthesis and Its Application in Fluorescence Imaging. *Org. Lett.* **2012**, *14*, 5912−5915.
(42) More, S.; Bhosale, R.; Choudhary, S.; Mateo-Alonso, A. Versatile 2,7-Substituted Pyrene Synthons for the Synthesis of Pyrene-Fused Azaacenes. *Org. Lett.* **2012**, *14*, 4170−4173.
(43) Frisch, M. J. et al., *Gaussian 09*, Revision A.01; Gaussian, Inc.: Wallingford, CT, 2009.
(44) Meyer, J. C.; Geim, A. K.; Katsnelson, M. I.; Novoselov, K. S.; Booth, T. J.; Roth, S. The structure of suspended graphene sheets. *Nature* **2007**, *446*, 60−63.
(45) Clar, E. Ein einfaches Prinzip des Aufbaues der aromatischen Kohlenwasserstoffe und ihrer Absorptionsspektren. *Ber. Dtsch. Chem. Ges. B* **1936**, *69*, 607−614.
(46) Clar, E.; Schoental, R. *Polycyclic Hydrocarbons*; Springer: London, 1964; Vol. *1*.
(47) Qian, G.; Zhong, Z.; Luo, M.; Yu, D.; Zhang, Z.; Ma, D.; Wang, Z. Y. Synthesis and Application of Thiadiazoloquinoxaline-Containing Chromophores as Dopants for Efficient Near-Infrared Organic Light-Emitting Diodes. *J. Phys. Chem. C* **2009**, *113*, 1589−1595.
(48) Gao, B.; Wang, M.; Cheng, Y.; Wang, L.; Jing, X.; Wang, F. yrazine-Containing Acene-Type Molecular Ribbons with up to 16 Rectilinearly Arranged Fused Aromatic Rings. *J. Am. Chem. Soc.* **2008**, *130*, 8297−8306.
(49) Brédas, J.-L. Mind the gap! *Mater. Horiz.* **2014**, *1*, 17−19.

DOI: 10.1021/jacs.9b01082
J. Am. Chem. Soc. 2019, 141, 5130−5134